Acta Neuropathologica Communications

CASE REPORT

Open Access

Dual phenotypes in recurrent astrocytoma, IDH-mutant; coexistence of IDH-mutant and IDH-wildtype components: a case report with genetic and epigenetic analysis

Junya Yamaguchi[1], Fumiharu Ohka[1*], Masafumi Seki[2], Kazuya Motomura[1], Shoichi Deguchi[1], Yoshiki Shiba[1], Yuka Okumura[2], Yuji Kibe[1], Hiroki Shimizu[1], Sachi Maeda[1], Yuhei Takido[1], Ryo Yamamoto[1], Akihiro Nakamura[1], Kennosuke Karube[2] and Ryuta Saito[1]

Abstract

Mutations in the isocitrate dehydrogenase (IDH) gene are recognized as the key drivers in the oncogenesis of astrocytoma and oligodendroglioma. However, the significance of IDH mutation in tumor maintenance and malignant transformation has not been elucidated. We encountered a unique case of IDH-mutant astrocytoma that, upon malignant transformation, presented two distinct intratumoral components: one IDH-wildtype and one IDH-mutant. The IDH-wild-type component exhibited histological findings similar to those of small cell-type glioblastoma with a higher Ki-67 index than the IDH-mutant component. Despite their genetic divergence, both components exhibited similar comprehensive methylation profiles within the CpG island and were classified into methylation class of "Astrocytoma, IDH-mutant; High Grade" by the German Cancer Center (DKFZ) classifier v11.4. Phylogenetic analysis demonstrated that the IDH-wildtype component emerged as a subclonal component of the primary tumor. Detailed molecular analyses revealed that the loss of the IDH mutation was induced by the hemizygous loss of the entire arm of chromosome 2, on which *IDH1* gene is located. Notably, the IDH-wild-type subclones uniquely acquired *CDKN2A/B* homozygous deletion and *PDGFRA* amplification, which is a marker of the aggressive phenotype of astrocytoma, IDH-mutant. Because these genetic abnormalities can drive oncogenic pathways, such as the PI3K/AKT/mTOR and RB signaling pathway, IDH-mutant gliomas that acquired these mutations were no longer dependent on the initial driver mutation, the IDH mutation. Molecular analysis of this unique case provides insight that in a subset of astrocytoma, IDH-mutant that acquired these genetic abnormalities, IDH mutation may not play a pivotal role in tumor growth and acquisition of these genetic abnormalities may contribute to the acquisition of resistance to IDH inhibitors.

Keywords Astrocytoma, Loss of IDH mutation, Methylation analysis, *PDGFRA* amplification, *CDKN2A/B* homozygous deletion

*Correspondence:
Fumiharu Ohka
ooka.fumiharu.j7@f.mail.nagoya-u.ac.jp
[1]Department of Neurosurgery, Nagoya University Graduate School of Medicine, 65 Tsurumai-cho, Showa- ku, Nagoya 466-8550, Japan
[2]Department of Pathology and Laboratory Medicine, Graduate School of Medicine, Nagoya University, 65 Tsurumai-cho, Showa-ku, Nagoya 466-8550, Japan

Introduction

Heterozygous mutations in the isocitrate dehydrogenase (IDH) genes are pivotal as driver mutations in the development of astrocytoma and oligodendroglioma [1, 2]. The mutant IDH produces the oncometabolite D-2-hydroxyglutarate by catalyzing α-ketoglutarate, which competitively inhibits histone demethylases, resulting in alterations in the genome-wide methylation profile [3]. While these methylation profile changes, induced by the mutant IDH, have been demonstrated to contribute to tumorigenesis, mutant IDH is suggested to be not important for malignant transformation. Recent human clinical trial revealed that IDH inhibitors inhibit the growth of IDH-mutant gliomas, indicating that mutant IDH plays pivotal roles even after the initial formation in IDH-mutant gliomas [4]. However, some case reports have described IDH-mutant gliomas losing the IDH mutation at recurrence. This indicates that presence of mutant IDH is not mandatory for recurrence [1, 5–7]. Thus, the significance of IDH mutation in tumor maintenance and malignant progression has not been elucidated.

In this report, we present a case of astrocytoma, IDH-mutant that included two distinct components: one that was more aggressive and lacking IDH mutation during malignant transformation, coexisting with an IDH-mutant component. Detailed genetic and epigenetic examinations were performed on the primary tumors and on both components of the recurrent samples to analyze the clonal evolution.

Clinical summary

A 34-year-old man with no relevant medical history presented with a seizure. An area of abnormal intensity in the left temporal lobe was identified by magnetic resonance image (MRI). The lesion exhibited high intensity on T2 weighted-images (WI), low intensity on T1WI, and no enhancement with gadolinium (Gd). Positron emission tomography showed high uptake of methionine in the lesion. Gross total resection (GTR) of the tumor was achieved using awake surgery, and the pathological diagnosis was astrocytoma, IDH-mutant grade 2, according to the WHO 2021 classification. The patient was monitored without additional treatment; however, recurrence was observed 34 months after the first surgery. We then performed a second surgery, achieving GTR once again. The pathological findings were similar to those obtained after the first resection. Despite continued observation without additional treatment, a recurrent lesion with Gd enhancement was found 19 months post second surgery. GTR was also achieved during the third surgery. The pathological diagnosis was astrocytoma, IDH-mutant grade 4 and glioblastoma, IDH-wildtype (detailed pathological findings are described below). Radiation therapy combined with oral temozolomide was administered, and the patient is presently under observation. A clinical summary is presented in Fig. 1.

Materials and methods

Immunohistochemical staining

The formalin-fixed paraffin-embedded (FFPE) samples were prepared per the standard protocol. Next, slides were mounted with 5-μm thick tissue sections and stained with hematoxylin and eosin. Multiple stainings were performed on the adjacent section with antibodies against IDH1 R132H (Dianova GmbH, H09 clone), GFAP (Dako, 6F2 clone), p53 (Santa Cruz Biotechnology, DO-1 clone), ATRX (Sigma-Aldrich, polyclonal), and Ki-67 (Dako, Mib-1 clone). All specimens were evaluated by two pathologists (S.M. and K.K.).

Extraction of genomic DNA

Genomic DNA (gDNA) was extracted from the buffy coat and frozen tumor specimens using a QIAamp DNA extraction kit (Qiagen, Hilden, Germany) or from unstained FFPE samples using a QIAamp DNA FFPE Kit (Qiagen, Hilden, Germany). The concentration of gDNA

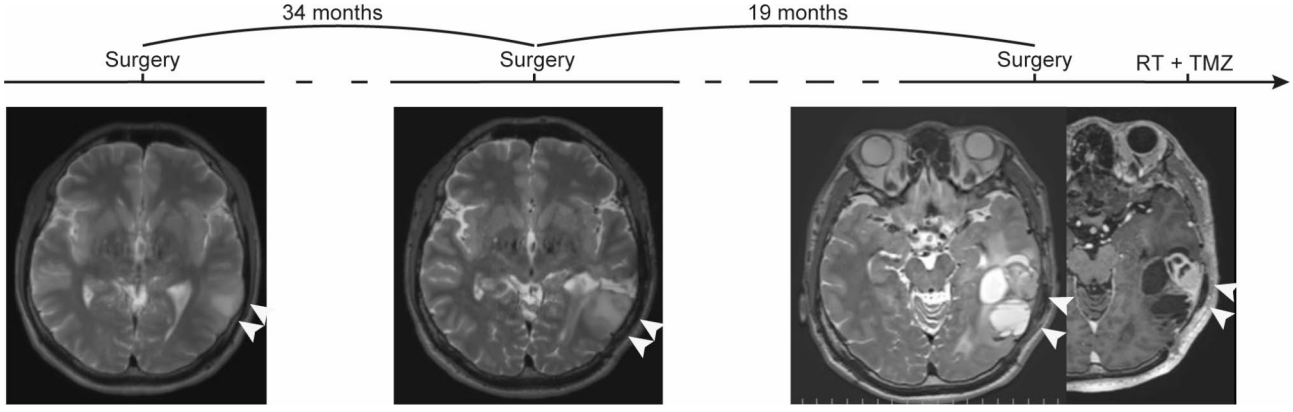

Fig. 1 Summary of clinical course of the patient. MRI sequences of T2-weighted image (T2WI) and gadolinium-enhanced T1-weighted image (T1WI) are shown. White arrows indicate abnormal lesions. RT, radiation therapy; TMZ, temozolomide

was determined using Qubit (Thermo Fisher Scientific, Waltham, MA, USA).

Sanger sequencing

For *IDH1* sequencing, we amplified a 129-bp fragment including codon 132. Polymerase chain reaction (PCR) was performed as follows: denaturation with 35 cycles at 95 ℃ for 30 seconds, annealing at 56 ℃ for 40 seconds, and extension at 72 ℃ for 50 seconds, with a final extension step at 72 ℃ for 7 minutes. The forward primer used was 5'-CGGTCTTCAGAGAAGCCATT-3', and the reverse primer was 5'-GCAAAATCACATTATTGCCAAC-3'. Sequence analysis was performed using ApE v2.0.60.

Whole exome sequencing (WES) and subsequent analysis

DNA libraries were prepared using the Agilent Sureselect V6 58 M according to the manufacturer's instructions. The NovaSeq6000 platform (Illumina, San Diego, CA, USA) was used for sequencing, and it generated 150-bp paired-end reads. FASTQ files were applied to the GENOMON pipeline and mutation calls were performed (https://genomon-project.github.io/GenomonPagesR/). Called mutations were sorted by the following criteria: Func.refGene = "exonic" or "splicing" or "exonic; splicing", misRate_tumor ≥ 0.05, misRate_normal < 0.02, P-value fisher_realignment > 1.1, variantPairNum_tumor ≥ 3, variantPairNum_normal < 3, strandRatio_tumor ≠ 1 & strandRatio_tumor ≠ 0. The sorted mutations are listed in Supplementary Table 1. The copy number analyses were performed using the Sequenza package [8]. The optimal phylogenetic tree was estimated using maximum parsimony and drawn using the bootstrap method in MEGA11 [9].

DNA methylation analysis

The Illumina Infinium Human Methylation EPIC BeadChip array (Illumina, San Diego, CA, USA) was utilized for a comprehensive genome-wide methylation analysis. gDNA, amounting to 600, was extracted from the FFPE samples. The preprocessing for the analysis of the EPIC array data and the computation of the beta score were performed with the Minfi package using R software, version 3.4.1 [10]. Following the application of the ChAMP package for filtering, the remaining probes for analysis amounted to 384,906 [11]. The beta scores were normalized using the BMIQ method in the ChAMP package. The top 5000 probes exhibiting the highest median absolute deviation on the CpG islands were selected for further analysis. The methylation profiles were analyzed with two-dimensional t-distributed stochastic neighbor embedding (t-SNE) in 2 dimensions using the Rtsne package. Reference methylation data for gliomas (GSE90496) were obtained from the Gene Expression Omnibus database (http://www.ncbi.nlm.nih.gov/geo/). A molecular classification algorithm and copy number analysis from the German Cancer Center (DKFZ classifier, https://www.molecularneuropathology.org/mnp) was performed [12]. In the copy number analysis by DKFZ classifier, a log2 ratio ± 0.4 was used as the cutoff for amplification/loss and a log2 ratio [13].

Public datasets analysis

For the analysis of public datasets, the cBioPortal for cancer genomics was utilized (https://www.cbioportal.org). Primary astrocytoma, IDH-mutant with CDKN2A/B homozygous deletion cases were collected ($n=15$) [1, 14, 15], and the published clinical outcomes were analyzed, and the published clinical outcomes were analyzed. Kaplan–Meier curves were drawn using Prism (version 9.3.1), and statistical differences were verified using a log-rank test.

Results

Pathological findings

On histopathological examination, tumor specimens obtained after the first and second resection exhibited diffuse infiltration of atypical astrocytic cells (the primary brain tumor is shown in Fig. 2A). Both tumors were positive for IDH1 R132H on immunohistochemistry (IHC) (Fig. 2A, inset) and had low mitotic activity. In the tumor specimen obtained at the third resection, two morphologically distinct brain tumor components were observed: one with abundant pleomorphic glial cells (NGY-R2A) and the other with abundant small round-cell tumor cells (NGY-R2B) (Fig. 2B). Microvascular proliferation was observed in both components. IHC revealed that NGY-R2A was positive for IDH1 R132H, while NGY-R2B was negative for IDH1 R132H (Fig. 2C). Both components were strongly positive for p53 and showed loss of expression of ATRX (Supplementary Fig. 1A and B). NGY-R2B cells showed a higher Ki-67 positivity rate (Fig. 2D) and a lower GFAP expression level than NGY-R2A cells (Supplementary Fig. 1C). Totally, NGY-R2B seemed to be more aggressive phenotype.

Molecular profiling

gDNA was meticulously extracted from two distinct areas (NGY-R2A and NGH-R2B) of the FFPE sample that was obtained during the third operation by micro-dissection. Sanger sequencing detected *IDH1* R132H mutation in the gDNA from NGY-R2A, but not from NGY-R2B (Supplementary Fig. 2A). Using WES data, we analyzed single nucleotide polymorphisms and copy number alterations (CNA) in each of the four samples. Phylogenetic tree analysis revealed that all samples shared the same origin, indicating that NGY-R2B was not a de novo clone but had transformed from a pre-existing IDH-mutant astrocytoma (Fig. 3A). Copy number analysis showed a

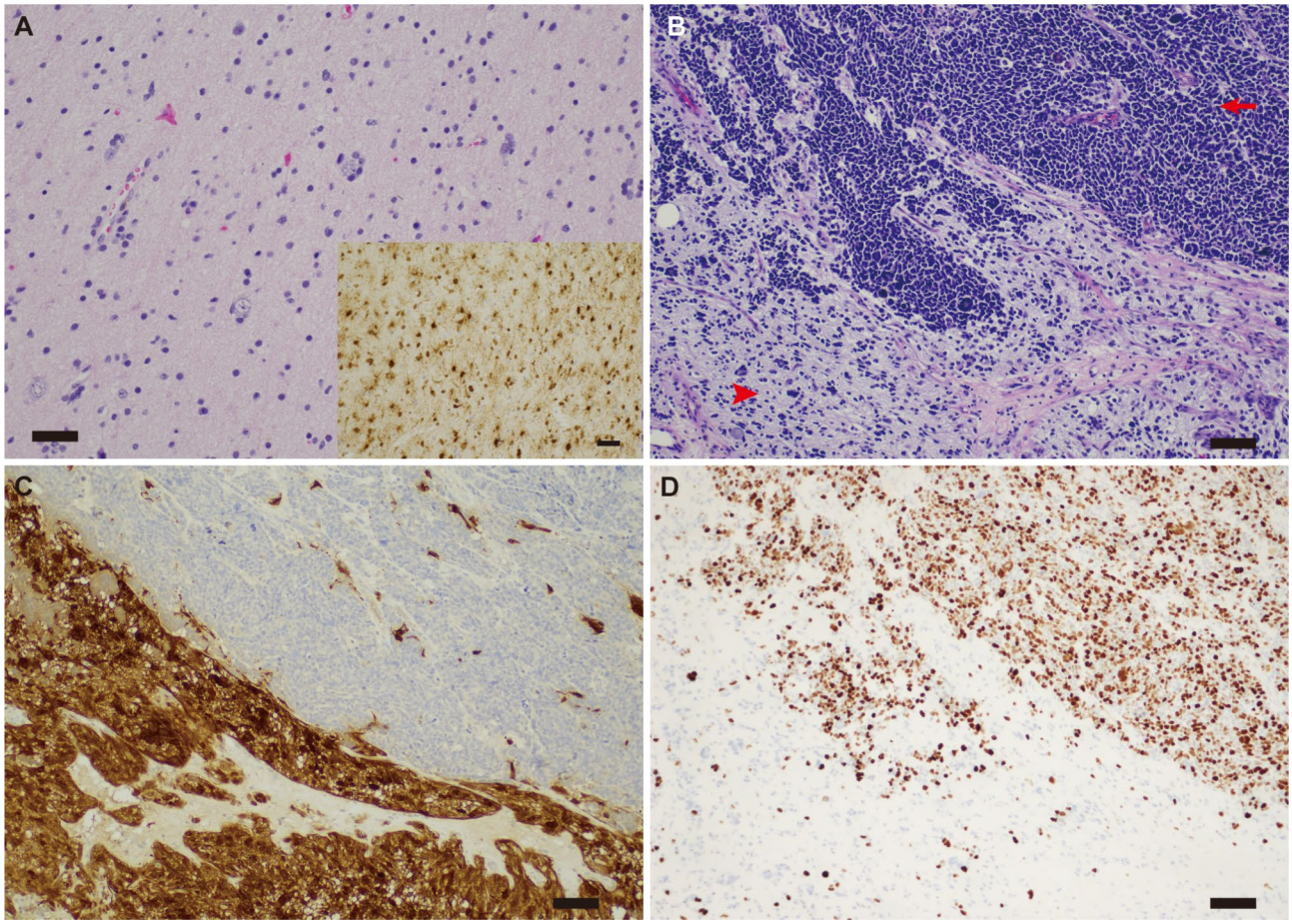

Fig. 2 Hematoxylin and eosin (HE) staining and immunohistochemistry (IHC) of the primary and the secondary recurrent tumor. (**A**) HE staining and IHC staining using anti-IDH1 R132H antibody (inset) of the primary brain tumor. (**B**) HE staining of the second recurrent tumor. The upper area of the image shows a small round-cell tumor component (arrow). Atypical glial cells with nuclear hyperchromasia and pleomorphism are observed in the lower area (arrowhead). (**C**) IHC staining of the second recurrent tumor with anti-IDH1 R132H antibody. (**D**) IHC staining of the second recurrent tumor using anti-Ki-67 antibody. All scale bars represent 100 μm

hemizygous loss of the entire arm of chromosome 2 containing *IDH1* locus (2q34), resulting in the loss of *IDH1* R132H mutant (Fig. 3B). Both NGY-R2A and NGY-R2B acquired CDKN2A/B homozygous deletions, and NGY-R2B additionally acquired PDGFRA amplification (Fig. 3A and supplementary Fig. 2B). These two copy number alterations were not detected in NGY-P and NGY-R1. Using published datasets, we found that astrocytoma with IDH mutation, *CDKN2A/B* homozygous deletion, and *PDGFRA* amplification had a significantly poorer prognosis than astrocytoma with only IDH mutation and *CDKN2A/B* homozygous deletion (Fig. 3C). This indicates that for IDH-mutant astrocytomas with CDKN2A/B homozygous deletion, acquisition of PDGFRA amplification plays a pivotal role in accelerating tumor growth. Consistent with this finding, NGY-R2B exhibited a more malignant histological phenotype than NGY-R2A. These findings suggest that while the mutant IDH plays a pivotal role in tumor formation via the induction of altered DNA methylation, additional driver gene alterations, such as *CDKN2A/B* HD and *PDGFRA* amplification, might play more important roles than IDH mutation in tumor growth.

Given that mutant IDH induces alterations in the comprehensive DNA methylation profile, we performed a methylation analysis for NGY-R2A and NGY-R2B. The *MGMT* promoter of both NGY-R2A and NGY-R2B were methylated (Estimated score=0.79786 [CI: 0.53427–0.93142] and 0.9166 [CI: 0.44925–0.99329], respectively; Fig. 3D) [16]. Using the German Cancer Center (DKFZ) classifier v11.4, NGY-R2A was classified into methylation class of "Astrocytoma, IDH-mutant; High Grade" with a calibrated score of 0.98. Although NGY-R2B was not classified, it achieved the highest calibrated score in the same category: "Astrocytoma, IDH-mutant; High Grade" with a score of 0.61 (Supplementary Fig. 2B) [12]. The t-distributed stochastic neighbor embedding (t-SNE) plot revealed that both NGY-R2A and NGY-R2B were

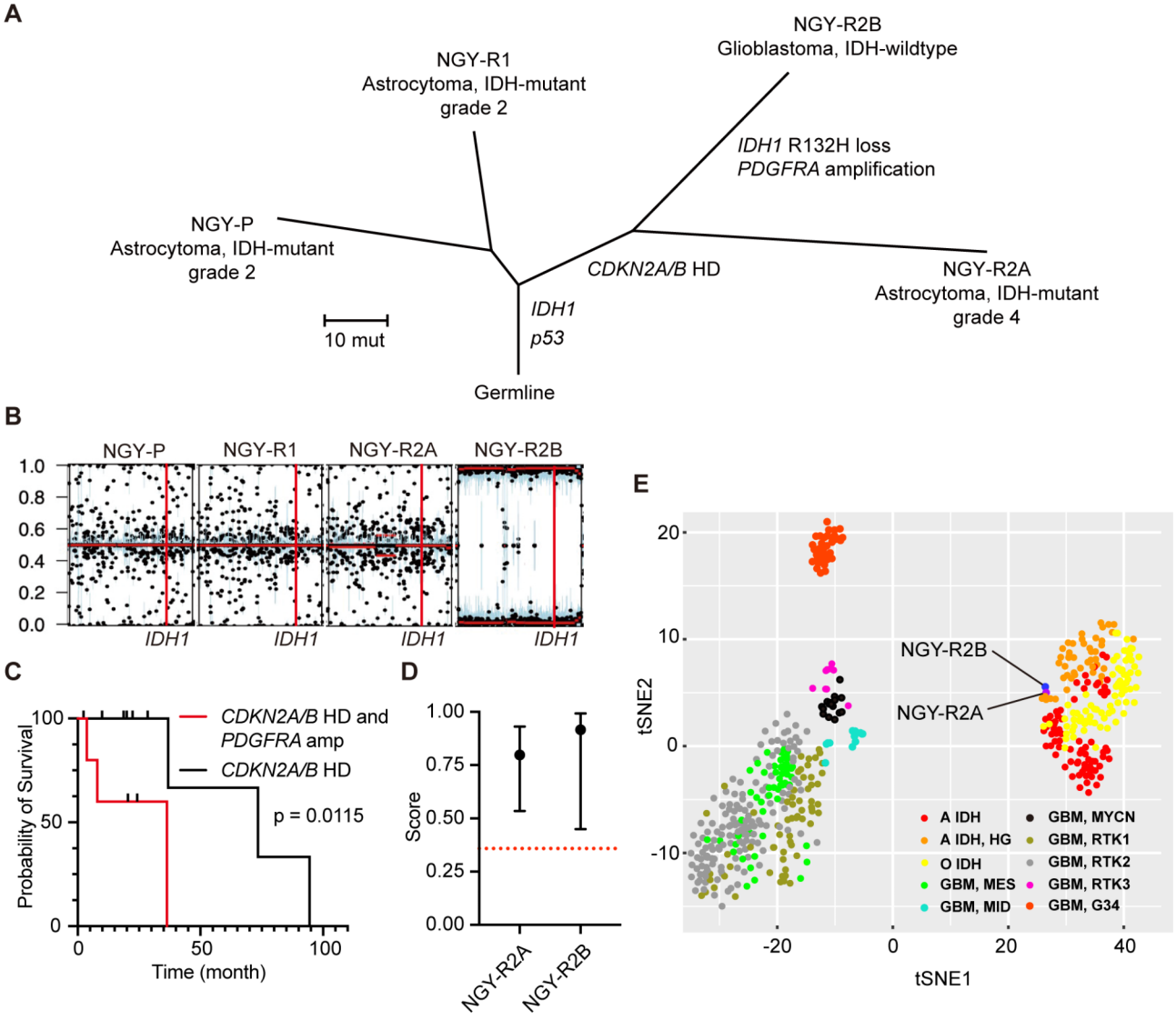

Fig. 3 Molecular profiling of NGY-P, NGY-R1, NGY-R2A, and NGY-R2B. (**A**) A phylogeny tree depicts the optimal evolution pattern of primary and recurrent samples highlighting genes that are frequently mutated in tumors. Branch lengths are proportional to the number of mutations detected. (**B**) This panels shows the β allele frequency of chromosome 2 for each sample, where the IDH1 are located. (**C**) Kaplan–Meier curves are used to represent cases with *CDKN2A* homozygous deletion (HD) and *PDGFR* amplification (amp; $n=5$), as well as cases with *CDKN2A* HD ($n=9$) among IDH-mutant astrocytoma. The X-axis indicates time (months) and the Y-axis indicates probability of survival. (**D**) *MGMT* promoter methylation status of NGY-R2A and NGY-R2B. The y-axis represents *MGMT* promoter methylation score, and the red dot line represents cut off value (0.3582). (**E**) t-distributed stochastic neighbor embedding (t-SNE) plot is drawn from the methylation data of our cases and reference data, which includes low-grade and high-grade gliomas. A IDH, IDH-mutant astrocytoma ($n=78$); A IDH HG, high-grade IDH-mutant astrocytoma ($n=46$); and O IDH, IDH-mutant oligodendroglioma ($n=80$). Reference methylation data for gliomas (GSE90496) were obtained from the Gene Expression Omnibus database (http://www.ncbi.nlm.nih.gov/geo/). A molecular classification algorithm and copy number analysis from the German Cancer Center (DKFZ classifier, https://www.molecularneuropathology.org/mnp) was performed [12]. GBM, MES ($n=56$), MID ($n=14$), MYCN ($n=16$), RTK1 ($n=64$), RTK2 ($n=143$), RTK3 ($n=13$), and G34 ($n=34$) represent GBM subgroups [12]

categorized as "High grade astrocytoma, IDH mutant" (Fig. 3E).

Discussion

We presented our experience of a rare case of astrocytoma, IDH-mutant that exhibited two distinct components histologically, each characterized by either IDH-wildtype or mutant IDH in the course of the malignant transformation. Although loss of IDH mutation at recurrence has been reported to occur in 6% of recurrent gliomas, this case was particularly noteworthy because the wildtype and mutant IDH components could be clearly distinguished histologically within the same recurrent specimen [17]. Of note, the components with IDH-wildtype revealed a higher Ki-67 index and cellularity compared with the adjacent component with the mutant IDH, which seemed to be a more

aggressive phenotype. Components with IDH-wildtype exhibited histological findings similar to those of small cell-type glioblastoma, a subtype of glioblastoma known for its poor prognosis [18].

First, we hypothesized that the methylation profile would shift to resemble that of a glioblastoma, IDH-wildtype; however, the methylation profile of this component was similar to that of high-grade IDH-mutant astrocytoma, as described in a previous report [6]. Although it was thought that IDH mutant cells might have been contaminated in the NGY-R2B sample, the IDH mutation was not called in whole exome sequencing, which could detect at least 2% VAF of IDH mutation, using the same DNA sample with the methylation analysis. Therefore, DNA derived from cells with the IDH mutation was not contaminated at least enough to affect methylation analysis. The methylation profile of the CpG island formed by the IDH mutation did not change even after loss of the IDH mutation. Notably, the methylation profile of the CpG island formed by the IDH mutation did not change even after loss of the IDH mutation. Considering the efficacy of the IDH inhibitor vorasidenib for grade 2 IDH-mutant glioma in the INDIGO trial, mutant IDH appears to play a pivotal role in the maintenance of grade 2 IDH-mutant glioma [4]. A phase 1/2 trial involving grade 2–4 IDH-mutant glioma demonstrated that the efficiency of the IDH inhibitor "DS-1001b" was worse for glioma with enhancing lesions than that for glioma without enhancing lesions, suggesting that during malignant transformation, tumor growth might be less dependent on mutant IDH [19]. In the present case, the second recurrent lesion was enhanced with Gd. There are few reports of detailed genetic analyses of cases with loss of IDH mutation at recurrence. Favero et al. reported a case of glioma with *PDGFRA* amplification, *CDKN2A/B* homozygous deletion, and loss of *IDH1* mutation at recurrence [7]. Acquisition of *CDKN2A/B* homozygous deletion at relapse occurs in 6% of recurrent gliomas, which is associated with an increase in proliferating neoplastic cells and active tumor growth [20, 21]. *CDKN2A/B* are involved in the retinoblastoma (RB) pathway, and it has been reported that the coexistence of CNAs that activate RB and PDGFR signaling pathway may critically promote tumor progression [22]. Using public database, we demonstrated that IDH-mutant glioma with *CDKN2A/B* homozygous deletion that acquired *PDGFRA* amplification have a worse prognosis. Because these genetic abnormalities can drive oncogenic pathways, such as the PI3K/AKT/mTOR and RB signaling pathway, IDH-mutant gliomas that acquired these mutations were no longer dependent on the initial driver mutation, the IDH mutation. In this case, when comparing two distinct components with or without IDH mutation developing from the same origin, the IDH-wildtype component with *CDKN2A/B* homozygous deletion and *PDGFRA* amplification exhibited a more aggressive phenotype than the IDH-mutant component with *CDKN2A/B* homozygous deletion. This supports that once astrocytoma, IDH-mutant acquire important genetic alterations such as *CDKN2A/B* homozygous deletion and *PDGFRA* amplification for malignant transformation, the IDH mutation might not be essential. Although further analyses of tumor specimens obtained from recurrent cases during IDH inhibitor treatment are needed, this may contribute to the acquisition of resistance to IDH inhibitors.

Conclusion

We presented a case of astrocytoma, IDH-mutant, exhibiting two distinct histological components, each characterized by either IDH-wildtype or mutant IDH, in the course of the malignant transformation. The findings obtained in this case are important for elucidating the mechanisms of resistance to IDH inhibitors, especially in the high grade astrocytoma, IDH-mutant. In malignant transformation, IDH-mutant glioma acquires additional important genetic alterations, such as *CDKN2A/B* homozygous deletion and *PDGFRA* amplification, thereby allowing the growth of malignant clones without IDH mutation.

Abbreviations

IDH	isocitrate dehydrogenase
MRI	magnetic resonance image
WI	weighted-image
Gd	gadolinium
GTR	gross total resection
WHO	world health organization
FFPE	formalin-fixed paraffin-embedded
gDNA	genomic DNA
PCR	polymerase chain reaction
WES	whole exome sequence
IHC	immunohistochemistry
CAN	copy number alterations
RB	retinoblastoma

Supplementary Information

The online version contains supplementary material available at https://doi.org/10.1186/s40478-024-01879-9.

Supplementary Material 1: **Supplementary Fig. 1**. (**A** and **B**) Immunohistochemical staining for p53 and ATRX at the second recurrence reveals that both components are strongly positive for p53 and negative for ATRX. (**C**) Immunohistochemical staining for GFAP at the second recurrence shows that the component with the glial cell tumor showed higher GFAP expression than the component with the small round cell tumor. All scale bars represent 100 μm.

Supplementary Material 2: **Supplementary Fig. 2**: (**A**) Sanger sequencing data of *IDH1* R132H, which showed dual peak in NGY-R2A but single peak in NGY-R2B (Red dotted rectangle) (**B**) Results of copy number analysis and methylation classification of NGY-R2A and NGY-R2B created by DKFZ classifier v11b4. NGY-R2A and NGY-R2B: two morphologically distinct brain tumor components, with abundant pleomorphic glial cells and the other with abundant small round-cell tumor cells, respectively.

Supplementary Material 3

Acknowledgements
Not applicable.

Author contributions
Conception and design: J.Y, F.O, K.M, K.K, and R.S; development of methodology: J.Y, F.O, M.S, K.M, K.K, and R.S; acquisition of data: J.Y, F.O, S.M, K.M, S.D, Y.S, Y.O, Y.K, H.S, S.M, Y.T, R.Y, A.N, K.K and R.S.; analysis and interpretation of data: J.Y, F.O, M.S, K.M, K.K, and R.S ; writing of the manuscript: J.Y and F.O.

Funding
This research was supported by AMED under Grant Number JP24ama221313 and JSPS KAKENHI Grant Number 23K08497.

Data availability
The datasets used and/or analysed during the current study available from the corresponding author on reasonable request.

Declarations

Ethics approval and consent to participate
This study was approved by the Institutional Review Board of Nagoya University Hospital (approval number: 2022-0043) and complied with all provisions of the World Medical Association Declaration of Helsinki. Informed consent was obtained from the patient for participation.

Consent for publication
Written informed consent was obtained from the patient.

Competing interests
The authors declare no competing interests.

Received: 3 September 2024 / Accepted: 19 October 2024
Published online: 26 October 2024

References

1. Johnson BE, Mazor T, Hong C et al (2014) Mutational analysis reveals the origin and therapy-driven evolution of recurrent glioma. Science 343(6167):189–193
2. Suzuki H, Aoki K, Chiba K et al (2015) Mutational landscape and clonal architecture in grade II and III gliomas. Nat Genet 47(5):458–468
3. Dang L, White DW, Gross S et al (2009) Cancer-associated IDH1 mutations produce 2-hydroxyglutarate. Nature 462(7274):739–744
4. Mellinghoff IK, van den Bent MJ, Blumenthal DT et al (2023) Vorasidenib in IDH1- or IDH2-Mutant low-Grade Glioma. N Engl J Med 389(7):589–601
5. Masui K, Onizuka H, Nitta M et al (2023) Recurrent high-grade astrocytoma with somatic mosaicism of isocitrate dehydrogenase gene mutation. Pathol Int 73(3):144–146
6. Mazor T, Chesnelong C, Pankov A et al (2017) Clonal expansion and epigenetic reprogramming following deletion or amplification of mutant IDH1. Proc Natl Acad Sci U S A;114(40):10743-8
7. Favero F, McGranahan N, Salm M et al (2015) Glioblastoma adaptation traced through decline of an IDH1 clonal driver and macro-evolution of a double-minute chromosome. Ann Oncol 26(5):880–887
8. Favero F, Joshi T, Marquard AM et al (2015) Sequenza: allele-specific copy number and mutation profiles from tumor sequencing data. Ann Oncol 26(1):64–70
9. Kumar S, Stecher G, Li M et al (2018) MEGA X: Molecular Evolutionary Genetics Analysis across Computing platforms. Mol Biol Evol 35(6):1547–1549
10. Aryee MJ, Jaffe AE, Corrada-Bravo H et al (2014) Minfi: a flexible and comprehensive Bioconductor package for the analysis of Infinium DNA methylation microarrays. Bioinformatics 30(10):1363–1369
11. Tian Y, Morris TJ, Webster AP et al (2017) ChAMP: updated methylation analysis pipeline for Illumina BeadChips. Bioinformatics;33(24):3982-4
12. Capper D, Jones DTW, Sill M et al (2018) DNA methylation-based classification of central nervous system tumours. Nature 555(7697):469–474
13. Capper D, Stichel D, Sahm F et al (2018) Practical implementation of DNA methylation and copy-number-based CNS tumor diagnostics: the Heidelberg experience. Acta Neuropathol 136(2):181–210
14. Barthel FP, Johnson KC, Varn FS et al (2019) Longitudinal molecular trajectories of diffuse glioma in adults. Nature 576(7785):112–120
15. Miller AM, Shah RH, Pentsova EI et al (2019) Tracking tumour evolution in glioma through liquid biopsies of cerebrospinal fluid. Nature 565(7741):654–658
16. Bady P, Delorenzi M, Hegi ME (2016) Sensitivity analysis of the MGMT-STP27 model and impact of genetic and epigenetic context to predict the MGMT methylation status in Gliomas and other tumors. J Mol Diagn 18(3):350–361
17. Lass U, Nümann A, von Eckardstein K et al (2012) Clonal analysis in recurrent astrocytic, oligoastrocytic and oligodendroglial tumors implicates IDH1-mutation as common tumor initiating event. PLoS ONE 7(7):e41298
18. Takeuchi H, Kitai R, Hosoda T et al (2016) Clinicopathologic features of small cell glioblastomas. J Neurooncol 127(2):337–344
19. Natsume A, Arakawa Y, Narita Y et al (2023) The first-in-human phase I study of a brain-penetrant mutant IDH1 inhibitor DS-1001 in patients with recurrent or progressive IDH1-mutant gliomas. Neuro Oncol 25(2):326–336
20. Varn FS, Johnson KC, Martinek J et al (2022) Glioma progression is shaped by genetic evolution and microenvironment interactions. Cell 185(12):2184–99e16
21. Shirahata M, Ono T, Stichel D et al (2018) Novel, improved grading system(s) for IDH-mutant astrocytic gliomas. Acta Neuropathol 136(1):153–166
22. Tateishi K, Miyake Y, Nakamura T et al (2023) Genetic alterations that deregulate RB and PDGFRA signaling pathways drive tumor progression in IDH2-mutant astrocytoma. Acta Neuropathol Commun 11(1):186

Publisher's note